LASER VIBROMETRY BASED DETECTIONS OF DELAMINATIONS IN AEROSPACE COMPOSITES

Yacine Amraoui, Nick Lieven
m.y.amraoui@bristol.ac.uk, nick.lieven@bristol.ac.uk
Dept. of Aerospace Engineering, University of Bristol, UK, BS8 1TR

Keywords : *Damage detection, Piezoelectric, Laser Doppler Vibrometry, Neural Networks*

Abstract

The significant progress in sensing and data processing technology has made monitoring and damage detection of engineering structures increasingly attractive. This paper presents a reliable in-situ damage detection technique, which is based upon dynamic analysis of a composite structure using a bonded piezo-ceramic patches as an actuators and a Scanning Laser Doppler Vibrometer as a sensor. In addition Neural Networks have been considered to be a viable tool for handling the large number of data. A multilayer perceptron (MLP) neural networks, was trained and tested using the slope, the y-intercept of the linear fit of the root mean square of the Frequency Response Function (FRF_{rms}) and the Deviation of the FRF_{rms} of a candidate composite structure.

1 Introduction

Composite materials offer enormous potential and benefits to the aerospace industry and many other sectors. However, composite laminates are susceptible to delamination from a wide variety of sources which include fabrication stress, environmental cyclic loading, handling damage, and foreign object impact damage. Delamination may lead to the severe degradation of the mechanical behaviour of structures due to the loss of structural integrity. The detection of delamination and the study of their effects on the mechanical behaviour of delaminated composite structures are important practical issues.

The purpose of structural health monitoring systems is to provide information about the condition of a structure in terms of reliability and safety before the damage threatens the mission objectives of the structure. In recent years, vibration based structural health monitoring using vibration based damage detection has been rapidly expanding and shown to be a feasible approach for detecting and locating damage. The philosophy behind this technique is that modal parameters -notably frequencies, mode shapes, and stiffness- change in a detectable manner due to degradation in the physical properties [1]. During the 1970s and 1980s, the aerospace industry made considerable effort to develop vibration-based damage detection methods in conjunction with the development of the space shuttle.

In summary, the review of the technical literature presented by Doebling *et al*. [2] shows an increasing number of research studies related to vibration-based damage detection. Numerous artificial neural network (ANN) techniques have been applied to structural health monitoring and damage detection [2,3]. Recent research indicates that neural networks, such as the radial basis function (RBF) and multi-layer back propagation (BP), can be trained on measured frequency responses of healthy and damaged specimens to recognise the actual condition of the structure. For instance, Chaudhry and Ganino [4] used measured Frequency Response Function (FRF) data over some specified frequency range as input to a BP neural network to identify the presence and severity of delamination in debonded beams. Although such work demonstrates the feasibility of training neural network on FRF data for damage detection, a very significant hurdle remains.

The size of the FRF data set is too large, which is determined by the number of spatial response locations and the number of spectral lines. The direct use of such data will lead to a very large number of input nodes to the neural network, which in turn will require a very large number of connections. Such neural networks remain impractical in terms of both training effort and convergence stability. However, Levin and Lieven [5] describe an alternative approach, based on modal parameter input. They reduce the size of the FRF data of a cantilevered beam by performing a modal analysis first, and applied a RBF neural, which was successful in detecting errors. Marwala and Hunt [6] studied a clamped beam using committee of multi-layer perceptron (MLP) network, which employs both modal properties and frequency response functions simultaneous-sly for the identification of faults. They conclude that the implementation of the multiple criterion method gives results that are more reliable than the results obtained when either frequency response approach or modal property approach is applied in isolation.

As mentioned earlier, the examples above highlight the need to find a more compact representation of the measured FRFs. A compressed technique derived from the work by castellini *et al.* [7] has been implemented in this paper. The rms.FRF, the slope of rms.FRF, and the deviation of the normalised FRFs have been used as a compact representation of the FRFs in order to train a MLP network to classify the delamination in composite structures.

2 Experimental Method

One of the principal failure modes in aerospace composites is the delamination of adjacent layers of pre-preg fibre layups. A fundamental requirement of the measurement technique is to excite the structure in the high frequency range (> 10 KHz), in order to reduce the wavelengths, increase curvatures and activate the gaping of the crack [8]. This requirement demands a very dense and a non-contacting measurement technique, which is attainable using a Scanning Laser Doppler Vibrometry for global assessment of delamination. As shown in fig. 1,

a dense meshing can be measured which corresponds to the candidate structure; localised geometry.

The method used here is to bond piezo-ceramic patches to the surfaces of the composite capable of excitation up to ~26 kHz. An Epoxy/Glass composite plate [45 90 -45 0 45 90 -45 0]$_s$ was used as a candidate structure as shown in fig. 2, which contained nine (9) delaminated areas, which were made by inserting small pieces of Teflon tapes at different layers during the layups.
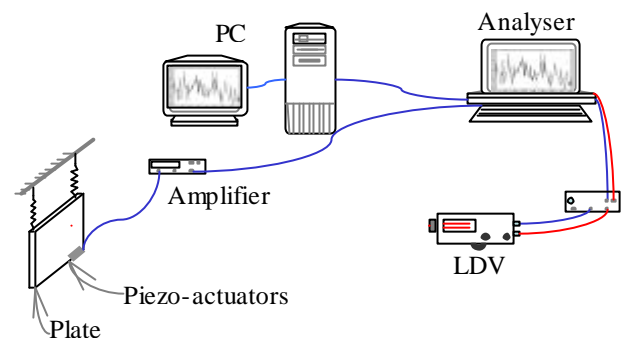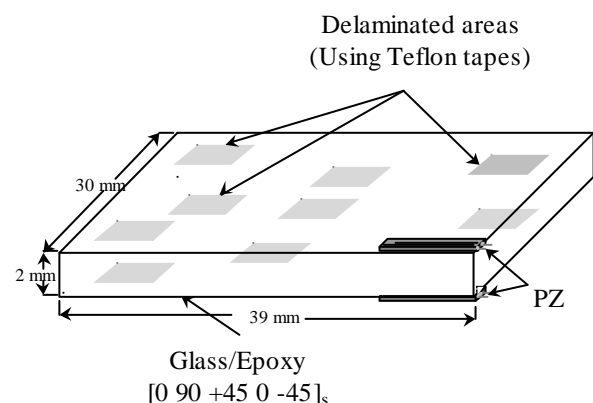

Fig. 1 Schematic of the experimental testing

Fig. 2 Delaminated Composite Plate

3 Piezoelectric materials

Piezoelectric actuators are non-contacting devices in the sense that they do not add any significant additional stiffness or mass to the structure. The basic principle is to excite the structure using the mechanical strain generated when an electric field is imposed to the piezo-actuator.

For a linear piezoelectric material, the relation between the electrical and mechanical variables can be described by linear relations [9]:

$$S_i = s_{ij}^E T_j + d_{mi} E_m \qquad (1)$$

$$D_m = d_{mi} T_i + e_{mk}^T E_k \qquad (2)$$

where:

$\{T\} = \{T_{11}\ T_{22}\ T_{33}\ T_{12}\ T_{13}\ T_{23}\}^T$, $\{E\} = \{E_1\ E_2\ E_3\}$
$\{S\} = \{S_{11}\ S_{22}\ S_{33}\ S_{12}\ S_{13}\ S_{23}\}^T$, and
$\{D\} = \{D_1\ D_2\ D_3\}$

The superscripts T and E signify that these quantities are measured at zero stress and constant field respectively.

The first equation describes the converse piezoelectric effect and the second equation describes the direct effect.

3.1 Piezoelectric Actuator

As shown in fig. 3, a number of assumptions must be made:

1. the patch of piezoelectric materials is assumed to be perfectly bonded to the surface of the plate;
2. the dimensions of the plate is infinite compared to the dimensions of the piezo-actuator;
3. the piezo-actuator induces a linear strain distribution in the in the plate; and
4. the strain energy in the actuator is equal to the strain energy induced in the plate by the actuator (conservation of the strain energy).
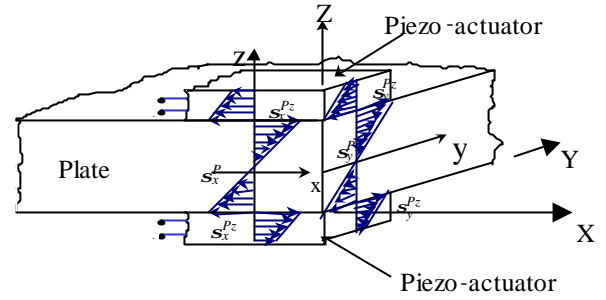

Fig. 3 Stress distribution in plate generated by bounded Piezo-Actuators

The magnitude of the strains induced by the piezo-actuator is a linear function of the applied voltage that can be expressed by [9]:

$$\bar{e}_x = \bar{e}_y = \frac{d_{31}}{t_{pz}} V_{pz} \qquad (3)$$

where d_{31} is the piezoelectric strain constant '1' is the induced strain direction and is perpendicular to the direction of the poling '3' and hence the applied field, t_{pz} is the piezo-actuator thickness and V_{33} is the applied voltage.

The piezoelectric actuator gives the added capability of applying a bending moment to the plate when an electric field is applied. Considering the free expansion of a piezoelectric plate element, the free strain due to the applied field, transforming this free strain to an applied stress required a two-dimensional Hooke' s Law.

$$d_{31}\bar{E} = \frac{s_x}{E_{pz}} - \frac{u_{pz} s_y}{E_{pz}} \qquad (4)$$

$$d_{31}\bar{E} = \frac{s_y}{E_{pz}} - \frac{u_p s_x}{E_{pz}} \qquad (5)$$

where u_{pz} is the Poisson's ratio of the piezoelectric lamina, $\bar{E}$ is the field strength in the 3rd direction and the subscripts x and y refer to the principal stresses in the plate directions of the piezoelectric actuator layer.

Equations (4) and (5) can be solved for the equivalent stress in the x and y directions applied to the piezoelectric actuator to produce the free piezoelectric strains to give :

$$\boldsymbol{s}_{pz} = \frac{E_{pz}d_{31}\overline{E}}{(1-\boldsymbol{u}_{pz})} \qquad (6)$$

4 Data processing

The experimental testing was carried out by applying a pseudo-random excitation force through Piezo-Actuators up to ~26 kHz, and using scanning laser doppler vibrometry in order to obtain a dense and accurate reading of the response. The simultaneous acquisition of force and response allows an FRF to be acquired at each geometric mesh location, as shown in fig. 4.
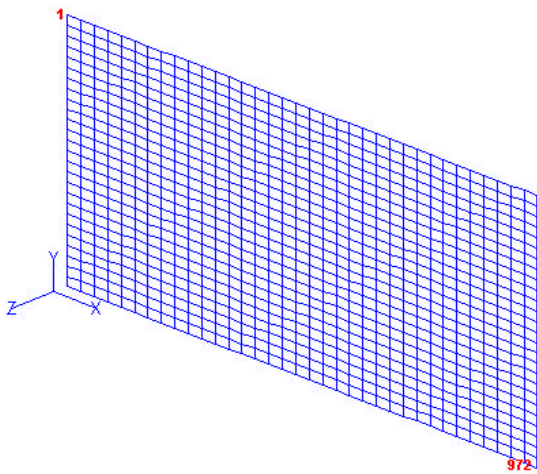

Fig. 4 Plate Mesh (972 nodes)

The FRFs obtained from modal testing have been normalised Eq.8, frequency-by-frequency in order to reduce dependence to resonance or anti-resonance peaks by dividing the FRFs by the α-trimmed average of the FRFs Eq.7, which reduce the effects of the extreme data. The trimmed mean is a modification of the arithmetic mean, means that both the top $\alpha\%$ and the bottom $\alpha\%$ of a ranked data set is

discarded and the mean is calculated for the rest of the sample. Therefor, the Trimmed Mean is $\alpha = \left(\dfrac{j}{n}\right)\%$, where n corresponds to the length of the array of the measured data (FRFs), and j is the number of data points discarded from each end of the original array.

$$FRF_{average}^{(j/n)}(\boldsymbol{w}) = \frac{1}{n-2j}\sum_{j+1}^{n-j}FRF_i(\boldsymbol{w}) \quad (7)$$

Therefore an elevated value should correspond to a high dynamic behaviour at defective points.

$$FRF_{norm_i}(\boldsymbol{w}) = \frac{FRF_i(\boldsymbol{w})}{FRF_{average}(\boldsymbol{w})} \qquad (8)$$

where $i = 1,2,...,972$ denotes the index relative to the nodes, and $\boldsymbol{w} = [0,26]\,kHz$.

According to the hypothesis of small damage, the normalised FRF should represent a reduced dependence whether by resonance or by anti-resonance peaks, therefore an elevated value should correspond to a high dynamic behaviour, i.e. to a defect. Figure 5 depicts a clear demonstration of the theory, the normalised FRFs correspond to a superficial defect with high amplitude, a deep defect and a non-defect with low amplitude and the excitation point with a very low amplitude.
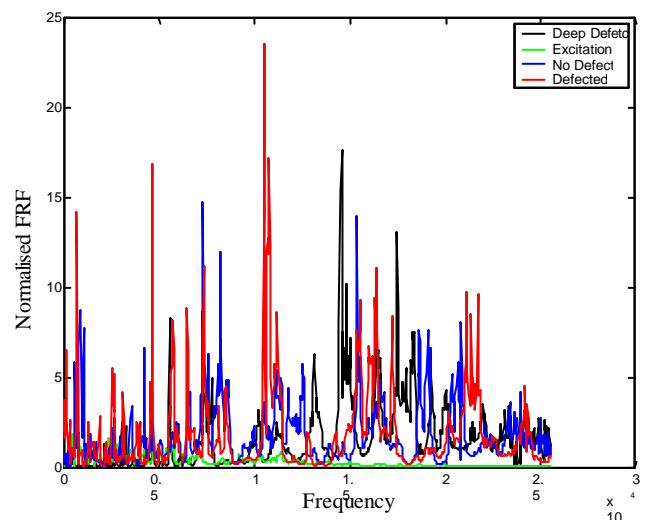

Fig. 5 Normalised FRFs

In order to simplify the processing procedure and reduce the amount of data without losses of information, the rms values of the FRFs in a limited number of frequency bands are calculated:

$$rmsFRF_i(k) = \sqrt{\frac{1}{\Delta w} \int_{(k-1)\Delta w}^{k\Delta w} FRF^2_{norm_i}(w)dw} \quad (9)$$

where k is the considered band and Δw is the integration range. The $rmsFRF_i(k)$ function is called the damage index as shown in fig. 6. It is clear that such rms values are an effective indicator of the defect. However, this technique is not entirely straightforward to use, as the discrimination capability is related to the analysis of several maps. For this reason, the $rmsFRF_i(k)$ can be simply interpolated by a linear curve fit using a least square algorithm in order to obtain a line representing the general trend of the amplitude values in each band, which gives the slope or the gradient a_i and m_i the y-intercept.

In general, non-defective points are characterised by a lower average level of the linear fitting with a negative slope while the defective points have higher average level with a negative slope depending on the depth, and the excitation points have a higher average level but a positive slope. However, there are some non-defective points have a negative slopes and such a cases can generate confusion with excitation points as shown in fig. 7 a,b.

In order to overcome this problem, the Standard Deviation DV_i of the $rmsFRF_i(k)$ was introduced by:

$$DV_i = \sqrt{\frac{\sum_{j=1}^{m}(rmsFRF_i(k) - m_i)^2}{m}} \quad (10)$$

where m is the number of frequency bands.

As shown in fig. 8 c, the defects in zones 1, 2 and 3 were clearly observable, which correspond to delaminations between layers 1-2,
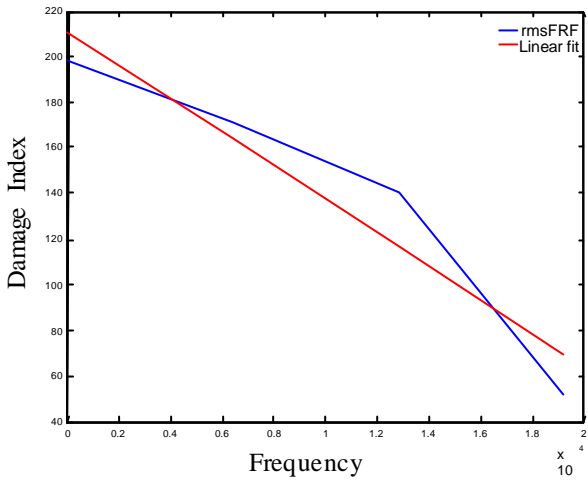
4-5, and 6-7 respectively. Unfortunately, the deep defects (i.e. between layers 8-9, 13-14, and 15-16) were not detected. However, the authors believed that a distributed high voltage piezo-actuators in the plate will correct the responses, which will activate the gaping of the deep cracks.
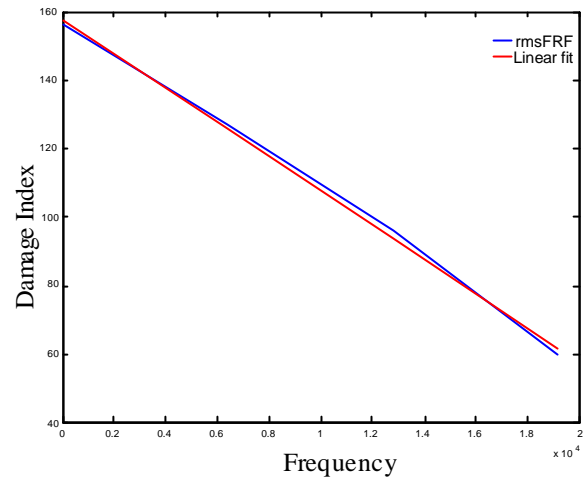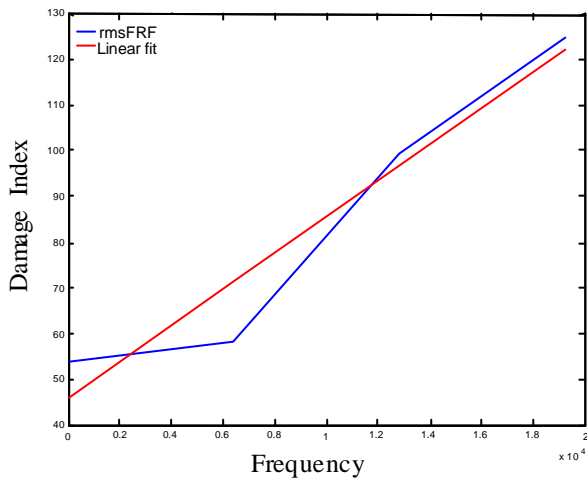

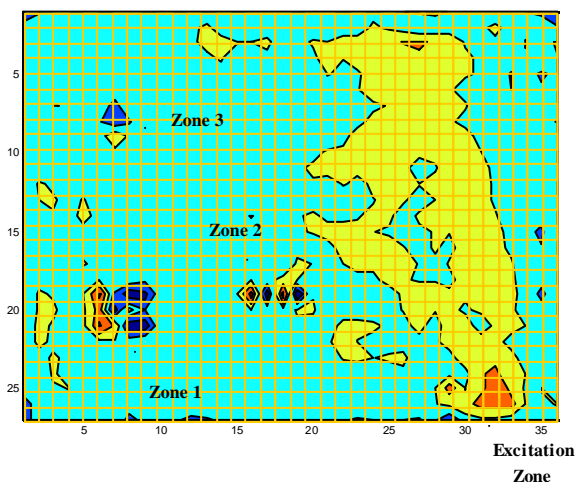**(a)** Non-delaminated zone
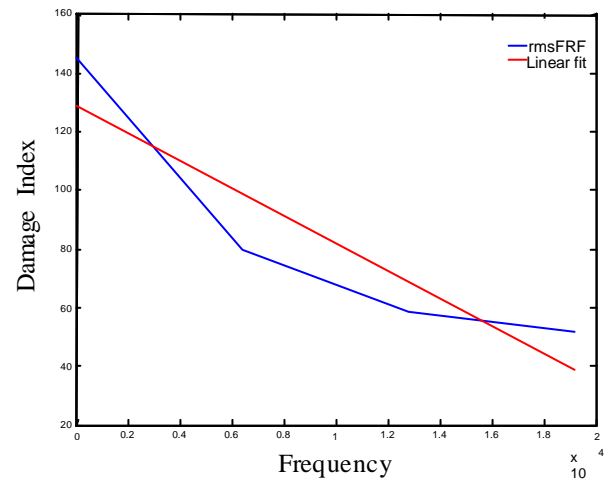
(b) Deep delaminated zone
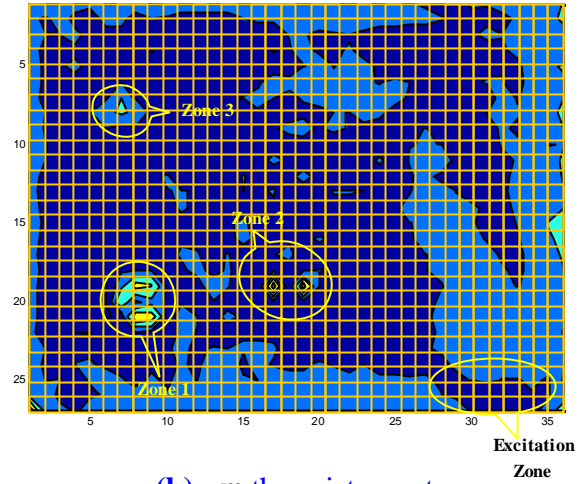
(c) Superficial delaminated zone

d) Excitation zone

Fig. 6 Damage Index

(a) The slope a_i

(b) m_i the y-intercept
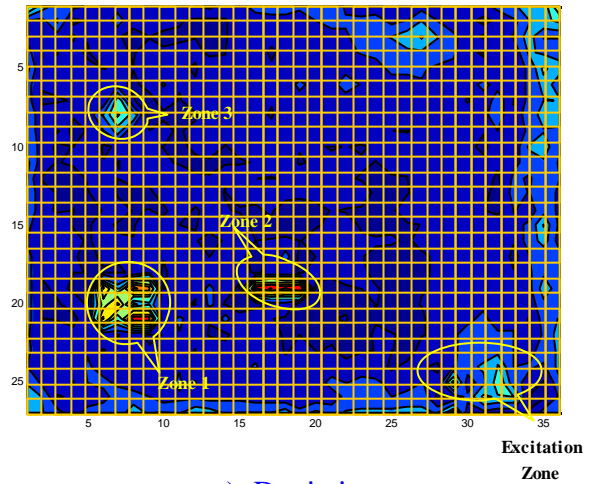
c) Deviation

Fig. 7 Maps of the slope α_i, μ_i, and the Deviation DV_i

5 Neural Networks

In this study, neural networks are viewed as parameterised graphs that make probabilistic assumptions about the data. Learning algorithms are viewed as methods for finding parameter values that look probable in light of the data. Learning processes occur by training the network through either supervised learning or unsupervised learning.

Unsupervised learning is used when only the input data are available. Supervised learning is used when the input and the output are available and neural networks are used to

approximate the functional mapping between the two. A supervised learning has been used in this study.

There are several types of neural network architectures, namely, multilayer perception (MLP) and radial basis function [10]. A MLP has been chosen because it provides a complex non-linear mapping between the input and the output. Figure 8 shows a schematic illustration of a typical MLP network.

Models of this form can approximate any continuous function to arbitrary accuracy if the number of hidden units NH is sufficiently large. If x is the output and y is the output, than non-linear mathematical relation that maps the input to the output may be written as follows [10]:

$$y_k(x) = b_k + \sum_{i=1}^{NH} w_{kj} \boldsymbol{f}\left(b_j + \sum_{j=1}^{NI} w_{ji} x_i \right) \quad (11)$$

Here b_k and b_j are bias parameters, NI is the number of input units and NH is the number of hidden units. The function $\boldsymbol{f}(\cdot)$ used was a sigmoid basis function and is defined as:

$$\boldsymbol{f}(x) = \frac{1}{1 + e^{-x}} \quad (12)$$

The error vector can be defined as being the difference between the network output and the desired output value.

$$E_k = d_k - y_k \quad (13)$$

Based on the error vector we can calculate the sum of squared vector as:

$$\boldsymbol{e} = \frac{1}{2} \sum_{k=1}^{NO} E_k^2 \quad (14)$$

Where NO is the number of output units.

This is the cost function to be minimised during the learning process. The sum-squared-error $\boldsymbol{e}$ is a function of all the variables of the network.
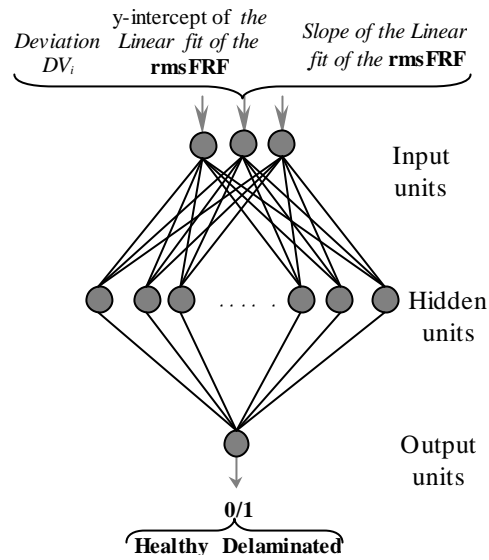

Fig. 8 MLP neural network (Classification)

In order to perform the training and the testing of the neural network, the candidate structure has been divided into two areas as shown in fig. 9.
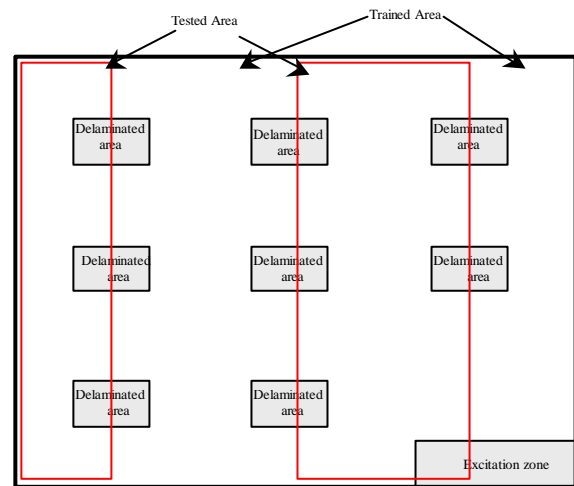

Fig. 9 Training and testing areas

The network used consists of three types of layers:
- the input layer that receives the compressed data ($\boldsymbol{a}_i$, $\boldsymbol{m}_i$ and DV_i) from the measured FRF;
- the hidden layer that provides the processing of the data; and

- the output layer that provides the result of the analysis, ie., healthy (0) or damaged (1)

One of the issues that has to be decided in configuring a back-propagation net is the hidden elements to be used. Therefore, different networks have been used. After 4500 learning cycles, a minimised error has been reached through a network contains 1200 set of neurons in the hidden layer using a 1GHz P? processor.

Figure 10 shows a plot of the sum square error *SSE* between the target and the output as a function of number of cycles that a data set was presented to the network, the training process has been stopped at a minimised value of the mean square error *MSE*=0.65637%, where the *Error*=8.101% . To validate the network a test process has been carried out using the input data from the testing area (see fig. 9) and the value of the mean square error was *MSE*=1.333% where the *Error*=11.545%, the authors believe that such error is acceptable.
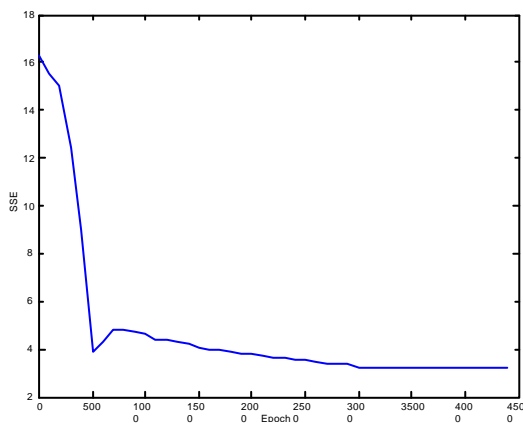

Fig. 10 Rate of convergence

6 Conclusion

The investigation carried out in this paper, gives us the ability of detection and discrimination of the overlapping defects in composite structures. Currently this technique is capable of detecting the superficial defects.

However, for the deep defects the authors believe that a distributed high voltages piezo-actuators on the structure may improve the sensitivity of the deviation and the deep defects could be detected.

The results obtained from the artificial neural network indicate that compressed data of the measured FRF provides a suitable methodology for damage detection.

References

[1] Adams RD, Cawley P, Pye C, Stone BJ. A Vibration Technique for non-destructively assessing the integrity of Structures, *Journal of Mechanical Engineering Science*, Vol.20, No 2, pp 93-100, 1978.

[2] Doebling SW, Farrar CR, Prime MB and Shevitz DW. *Damage Identification and Health Monitoring of Structural and Mechanical Systems from Changes in their Vibration Characteristics.* A Literature Review, Los Alamos National Laboratory report LA-13070-MS, 1996.

[3] Zeng P. Neural Computing in Mechanics. *Applied Mechanics Reviews*. Vol. 51, pp 173-197, 1989.

[4] Chandhry Z and Ganino AJ. Damage Detection using Neural Networks - an initial experimental study on debonded beams. *Journal of Intelligent Material Systems and Structures*, Vol. 5, pp 585-589, 1994.

[5] Liven RI and Lieven NAJ. Dynamic Finite Element Model updating using Neural Networks. *Journal of Sound and Vibration*, Vol. 210, pp 593-607, 1998.

[6] Marwala T and Hunt HEM. Fault Identification using Finite Element Models and Neural Networks. *Mechanical Systems and Signal Processing*, Vol. 13, pp 475-490, 1999.

[7] Castellini P, Revel GM and Scalise L. Diagnostic of Composite Materials by Laser Techniques: Application on panels with different structures and shapes. *Proceeding of IMAC XIX: A conference on Structural Dynamics*, Hyatt Orlando Kissimmee Florida, Vol. 1, pp 710-716,2001.

[8] Dugundji J. Simple Expressions for Higher Vibration Modes of uniform Euler Beams. *AIAA Journal*, pp 1013-1014, 1988.

[9] An American National Standard. *IEEE Standard on Piezoelectricity*, ANSI/IEEE Std 176, 1987.

[10] Bishop C.M. Neural Networks for Pattern Recognition. Oxford University Press Inc., ISBN 0-19-853864-2, 1995.